Acta Geotechnica (2018) 13:1203–1213
https://doi.org/10.1007/s11440-018-0637-6

RESEARCH PAPER

# Freezing of water confined in porous materials: role of adsorption and unfreezable threshold

**Chao Zhang**[1] · **Zhen Liu**[1]

Received: 21 December 2016 / Accepted: 30 January 2018 / Published online: 14 February 2018

## Abstract

It has been widely accepted in scientific communities that water confined in porous materials gradually freezes from large pores to small pores at subfreezing temperatures ($< 0$ °C), though we still describe a soil as frozen or unfrozen in engineering practice and daily life. Therefore, it is more accurate to say "how frozen" instead of "whether frozen." This gradual freezing process is temperature-dependent because water in pores of different sizes has different energy levels, which requires different temperatures for its phase transition, leading to a relationship between unfrozen water content and temperature in soils. However, the understanding of this relationship, i.e., the Phase Composition Curves (PCC), is still incomplete, especially in the low-temperature range. We still lack answers to even the most fundamental questions for frozen soils and their PCCs: (1) How much pore water could be frozen? (2) How do capillarity and adsorption control the freezing of pore water? This study investigates two basic physical mechanisms, i.e., unfreezable threshold and adsorption, for their dominant roles in the low-temperature range of the PCC. To quantify the effects of the unfreezable threshold, molecular dynamics simulation was employed to identify the unfreezable threshold of cylindrical pores. The simulation results, for the first time, revealed that the unfreezable threshold corresponds to a pore diameter of $2.3 \pm 0.1$ nm and is independent of the wettability of the solid substrates. Combining this unfreezable threshold with a modified Gibbs–Thomson equation, a mathematical model was proposed to predict the melting temperature in pores of different sizes, which considers both unfreezable threshold and adsorption. Comparisons of the results calculated with the new model and other two conventional equations against experimental results indicated that the model can improve conventional equations which have been used for centuries by including the two mechanisms, which significantly improved our understanding of frozen soils.

**Keywords** Adsorption · Frozen soils · Molecular dynamics · Nano-size pores · Temperature depression · Unfreezable threshold

## 1 Introduction

The pores permeating porous materials place significant confinement effects on the pore water, substantially differing its phase transition behavior from pure bulk water [1]. As a result, a considerable amount of pore water remains unfrozen in porous materials under the freezing point of pure bulk water, frequently referred as the temperature depression effect. This depression effect is significant in many aspects of material sciences, soil physics, and geotechnical engineering, such as characterization of mesoporous materials [44], environmental issues induced by permafrost thawing and frost heaving [47]. In geotechnical engineering practice, the freezing of pore water may significantly impact the soil strength and hydraulic conductivity [41], rendering frost action is an inevitable concern for civil engineers in cold regions [30].

The Phase Composition Curve (PCC) is the relationship between unfrozen water content and temperature in frozen soils, which is a basic constitutive relationship in modeling

---

✉ Zhen Liu
zhenl@mtu.edu

Chao Zhang
chao@mtu.edu

[1] Department of Civil and Environmental Engineering, Michigan Technological University, Houghton, MI 49931, USA

frozen porous materials. The PCC is a cornerstone in defining the thermodynamic states of frozen soils and thus a theoretical tool to investigate complex mechanical behavior, e.g., creep (e.g., Liao et al. [27], Xu et al. [59], and Zhao et al. [66]), plasticity (e.g., Borja [7]) and heterogeneity (e.g., Ma et al. [33], Song and Borja [50], Song and Borja [51], and Borja et al. [8]). Therefore, it is indispensable to develop the PCC based on complete physical mechanisms covering the full range of temperature.

The major physical mechanism underlying the temperature depression effect is the variation of the water potential and its components, which stems from the water–mineral interaction within porous materials [25, 30]. Considerable research efforts have been made to construct the PCCs for soils and could be classified into three primary procedures. In the first procedure, the PCCs are formulated via combining the matric suction–temperature depression relationship and the unfrozen water content–matric suction relationship [24, 41, 52]. The former relationship is usually represented by different forms of the Clapeyron equation [22, 23, 25, 48, 57, 61]. The latter relationship is sometimes referred as the Soil Freezing Characteristic Curve (SFCC) [24]. The SFCC is analogous to the Soil Water Characteristic Curve (SWCC) [24, 52], a fundamental concept in unsaturated soils, which describes the relationship between the water content and the matric suction in unfrozen soils. This is because freezing and drying involve a similar physical process in which the liquid water retained in the soil matrix is replaced by another phase, i.e., ice in freezing and air in drying [9, 25]. As a result, the SWCC is usually used to approximate the SFCC in practice. In the high suction range of the SWCC, adsorption becomes manifest and may dominate the matric suction, prevailing over capillarity [31]. However, the adsorption effect has not been well considered in the conventional SWCC models [28, 58]. Hence, this procedure may not be able to capture soil freezing characteristics in the high suction range, which corresponds to the low-temperature range. In the second procedure, porous materials are represented by a bundle of capillary tubes utilizing the concept of the bundle of cylindrical capillary (BCC) model [29]. Then, the PCCs of porous materials can be transformed into the phase composition behavior of a series of cylindrical tubes with different diameters. The Clapeyron equation is employed for the matric suction–temperature depression effect, while the Young–Laplace equation is used to determine the suction in the capillary tubes. Evidently, adsorption, which dominates the suction in small pores, is excluded in this formulation. In the third procedure, the BCC model is also chosen to conceptualize the porous materials. However, the temperature depression effect is directly determined from the pore diameter through the Gibbs–Thomson relationship [15, 57]. Adsorption is also excluded in this procedure, indicating the possible inaccuracy in minuscule size pores. Therefore, to date, there has been no widely accepted procedure to develop the PCCs for soils, and the adsorption effect has not been well considered in these existing procedures.

The freezing of water confined in pores is the basis for interpreting the PCCs of porous materials. This study is focused on the freezing of pore water confined in nanoscale pores, which corresponds to the low-temperature range of the PCCs. Especially, this study will answer two fundamental questions about the behavior of frozen porous materials: how “frozen” a porous material could be and the influence of adsorption on the phase change of pore water. In Sect. 2, the physical mechanisms underlying the adsorption effect are analyzed in terms of free energy concepts, and another physical mechanism, i.e., the existence of an unfreezable threshold, is revealed. In Sects. 3 and 4, molecular dynamics simulation is employed to investigate the unfreezable threshold in cylindrical pores. At last, a novel mathematical model based on the modified Gibbs–Thomson equation incorporating adsorption and the unfreezable threshold is proposed to describe the phase behavior of the water confined in cylindrical pores.

## 2 Adsorption and unfreezable threshold

The freezing temperature depression can be understood from a viewpoint of free energy. In an equilibrium system, the chemical potentials of water and ice across the water–ice interface should satisfy [16]:

$$\mu_{\mathrm{w}}(T,P) = \mu_{\mathrm{i}}(T,P) \tag{1}$$

where $\mu_{\mathrm{w}}$ and $\mu_{\mathrm{i}}$ are the chemical potentials of water and ice, respectively; and $T$ and $P$ are the temperature and pressure for defining the thermodynamic state of the system, respectively. The chemical potential is a measure of the free energy of each substance and defined as the partial molar free energy. For pure bulk water, at $T = 273.15$ K and $P = 1$ atm, the chemical potential of water equals to that of ice. Accordingly, Eq. 1 is satisfied, and water and ice are in coexistence. The chemical potential of ice becomes smaller than that of unfrozen water at $T < 273.15$ K and $P = 1$ atm, indicating that the ice phase is more stable than the liquid phase [16]. Therefore, pure bulk water will transform into ice when the temperature decreases below 273.15 K. For water confined in pores, however, the free energy of water will be altered by the confinements, so will be the ice confined in the pore, leading to the temperature depression effect. In 1935, Schofield [45] probably firstly reported that the freezing temperature depression is directly related to the free energy difference between pore water and pure bulk water. Under this premise, the temperature depression effect can be expressed as a function of this free energy difference according to the Clapeyron equation [25, 29]. This free energy difference is usually quantified through the water potential which is defined as the difference between the partial volume free energies of water retained in the solid matrix and pure bulk water [40]. The water potential equals the matric potential under the conditions of no impurities and negligible gravitational effects. The matric suction is the negative of matric potential and more frequently used in geotechnical engineering. The freezing temperature depression effect can be expressed as a function of matric suction via the Clapeyron equation as [22, 23, 29, 57]:

$$T_{\mathrm{m}} = T_0 \exp\left(\frac{\psi}{-\rho_{\mathrm{w}} L_{\mathrm{a}}}\right) \tag{2}$$

where $T_0$ is the freezing temperature of pure bulk water, i.e., 273.15 K; $\psi$ is the matric suction; $\rho_{\mathrm{w}}$ is the density of water; $L_{\mathrm{a}}$ is the latent heat of water fusion.

There are mainly two physical mechanisms contributing to the matric suction: adsorption via surface forces and capillarity via surface tensions. The Young–Laplace equation is widely used to calculate the matric suction ($\psi$) induced by capillarity and can be expressed as [26, 60]:

$$\psi = 2T_{\mathrm{s}}\kappa \tag{3}$$

where $T_{\mathrm{s}}$ is the surface tension of the water–ice or water–vapor interface, and $\kappa$ is the curvature. As introduced above, capillarity is considered as the dominant mechanism, while adsorption is missing in the conventional theories for the phase change of pore water. However, this presumption may not apply especially to the nano-size pores. For example, Schofield [45] pointed that the capillary potential may not apply to clayey soils in which nano-size pores are prevalent. The relationship between the matric suction and pore diameter ($D$) is conceptually illustrated in Fig. 1, in which difference between the prediction by the Young–Laplace equation [Eq. (3)] and the real matric suction is schematically illustrated. In general, the matric suction increases as the pore diameter decreases, indicating that a smaller pore can provide a greater confinement effect. In large pores (approximately $D \geq 10$ nm), surface tension is the dominant factor in lowering the free energy of pore water, and correspondingly, the matric suction can be well interpreted using capillarity. In small pores (approximately $3\ \mathrm{nm} < D<10\ \mathrm{nm}$), the thickness of the adsorptive water film is comparable to the pore diameter, and as a result, the contribution of adsorption becomes manifest. In this range, an estimation of the matric suction using only capillarity may cause considerable errors. In minuscule pores (approximately $D \leq 3$ nm), the size of water molecules is comparable to the pore diameter, and thus, the pore water cannot be treated as a continuum anymore. Instead, most of the pore water exists as adsorptive water and behaves as discrete molecular layers. Most of the water molecules stay in the range of surface forces, and consequently, the matric suction is dominated by adsorption rather than capillarity. The Young–Laplace equation tends to underestimate the matric suction in such small pores significantly.

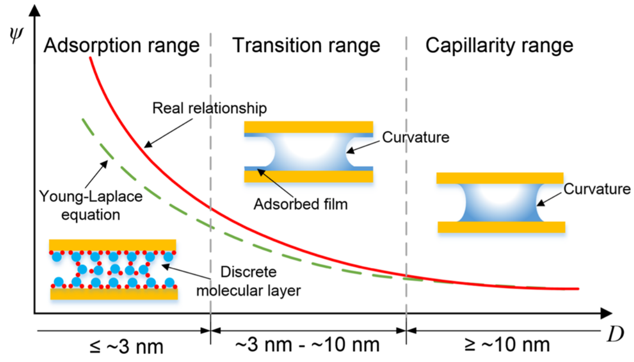

**Fig. 1** Matric suction in nano-size pores: the interplay between adsorption and capillarity

According to the Clapeyron equation, a lower temperature indicates a higher suction, which is associated with smaller pores. Therefore, the low temperatures correspond to the nano-size pores. In these pores, adsorption is substantial and thus should be well considered for the low-temperature range of the PCCs. The density and structure of adsorptive water differ from those of pure bulk water and capillary water [35]. As observed in Zhang et al. [62], surface forces will arrange adsorptive water into some regular molecular layers in some orders. For these ordered water molecules, more energy is required to rearrange the water molecules into ice [35]. It is thus more difficult to transform them into ice. As a result, it is postulated that adsorptive water cannot form regular ice structures [35]. As illustrated in Fig. 1, water confined in the minuscule pores (approximately $D \leq 3$ nm) is significantly influenced by the surface forces and is rearranged into ordered discrete molecular layers, suggesting that all the confined water can be regarded as adsorptive water. This water confined in minuscule pores can only form some nanocrystals but not regular ice crystals. The existence of this phenomenon has been confirmed by experimental and simulation observations on nano-size pores (e.g., Findenegg et al. [12], Koga et al. [21], and Shiomi et al. [49]). Therefore, there exists a range of pore diameter where all the pore water is adsorptive water and cannot form regular ice structures. This range of pore diameter is referred as “unfreezable region,” whereas its upper boundary is referred as “unfreezable threshold” in this study. While the existence of the unfreezable threshold has been postulated, to date, no research on this unfreezable threshold has been reported.

However, this can totally change our understanding of pore water and frozen porous materials.

This study targets at accurately quantifying the unfreezable threshold and incorporating the unfreezable threshold and adsorption in the formulation of the PCCs. Some experimental results are already available and will be used to quantify the adsorption effect (e.g., Morishige [39], Schreiber et al. [46], and Findenegg et al. [12]). Notwithstanding, to the authors' best knowledge, the unfreezable threshold has not received enough experimental or simulation efforts yet. Molecular dynamics has been proved to be an efficient tool to investigate the freezing of water (e.g., Koga et al. [21], Moore and Molinero [37], Gonzalez Solveyra et al. [13], and Moore et al. [38]). Also, MD has been successfully used to address soil behavior and properties (e.g., Katti et al. [19, 20], Amarasinghe and Anandarajah [2], Anandarajah and Amarasinghe [3], Zhang et al. [64, 65]). Herein, MD was chosen as a tool to understand the freezing of water confined in minuscule pores, i.e., $D < 3$ nm, and a series of MD simulations was conducted to determine the unfreezable threshold accurately.

## 3 Models and methodology

### 3.1 Molecular models

To investigate the unfreezable threshold, the freezing of water confined in the cylindrical nano-size pores was simulated using MD. As shown in Fig. 2, a water-pore system, including a cylindrical pore and water molecules, is selected for this purpose. The dimensions of the simulation cell are $6D \times (D + 10\ \text{Å}) \times (D + 10\ \text{Å})$ at the *x*-, *y*-, and *z*-directions. The solid around the cylindrical pore exhibits a Face-Centered Cubic (FCC) crystal structure (shown in Fig. 2c). The reason for choosing the FCC crystal structure is its widespread application in molecular simulations for representing general elastic solids, e.g., Luan and Robbins [32], Cheng and Robbins [10], and Zhang et al. [63]. The primary goal of molecular simulations herein is to provide a theoretical value for the unfreezable threshold for nano-size pores. Therefore, the generality of the FCC crystal structure will enable the results to be easily transferable to other cases. The lattice constants of the FCC crystal, i.e., *a*, *b*, and *c*, are 4.0 Å. At the center of the solid substrate, a cylindrical pore is carved with a diameter of *D*. The pore diameter (*D*) varies from 2.0 to 3.0 nm with an interval of 0.2 nm to determine the unfreezable threshold. The pore is thereafter filled with water molecules, and the length of the pore water cylinder was set as 4*D*, 2*D* smaller than the total length of the pore to reserve extra space for freezing expansions. The Packing Optimization for Molecular Dynamics Simulations (PACKMOL) [34] was utilized to generate the initial configuration of the water cylinder. The diameter of the water cylinder is 3.1 Å smaller than the pore diameter (*D*) to avoid segmentation errors. The number of water molecules in the water cylinder was calculated to ensure

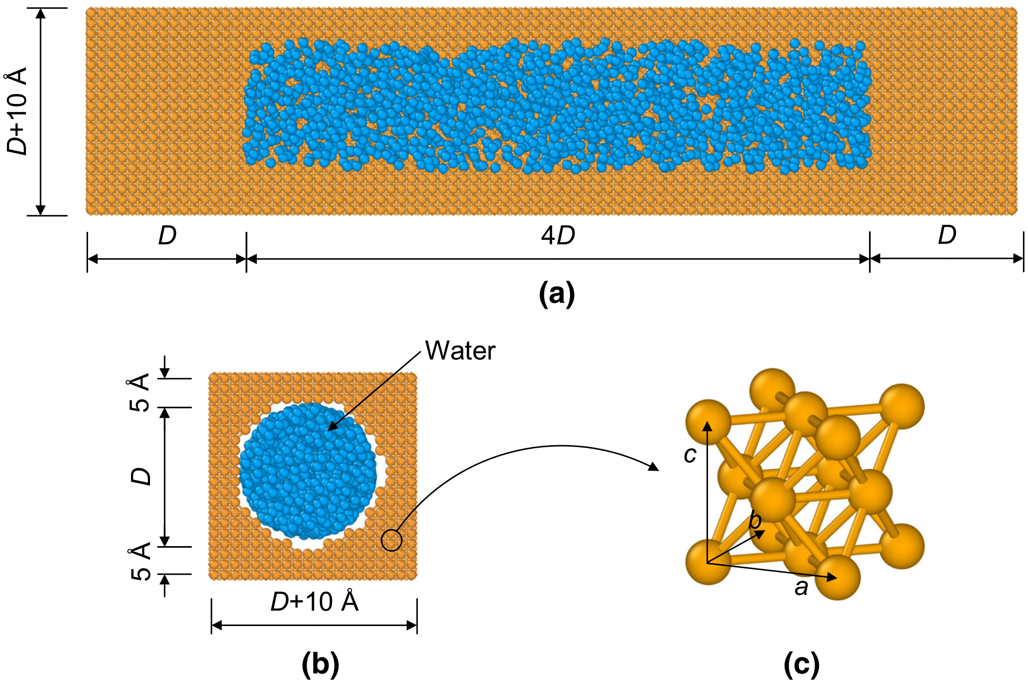

**Fig. 2** Molecular models (yellow: solid atom; blue: water molecule) of the water confined in pores: **a**, **b** cross-sectional views of initial configurations; **c** FCC crystal structure of the solid. Lattice constants a, b, and c are 4.0 Å (color figure online)

that the density of the pore water is identical to that of pure bulk water.

## 3.2 Interatomic potentials

In the MD simulation, the interactions between atoms in the molecular models were determined by the interatomic potentials. In the water-pore system shown in Fig. 2, there are two types of particles, i.e., solid atoms and water molecules. Hence, the interatomic potential between any two particles should be well defined. As a result, three types of interatomic potentials need to be considered: water–water interaction, solid–solid interaction, and solid–water interaction.

The water–water interaction was modeled using a water model, and many water models have been proposed for this purpose (e.g., Berendsen et al. [6], Berendsen et al. [5], and Jorgensen and Tirado-Rives [18]). The computational cost is one of the biggest obstacles to the application of MD simulations, limiting both temporal and spatial scales of simulation systems. Specifically for freezing simulations, a relatively large timescale, i.e., hundreds of nanoseconds, is required for producing stable ice crystals. When adopting conventional atomistic water models, this timescale indicates unpractical computational costs due to the particle–particle, particle–mesh (PPPM) [14] calculation of long-range Coulombic forces. Therefore, the monoatomic water (mW) model proposed by Molinero and Moore [36], a coarse-grained water model, rather than conventional atomistic water models was selected to describe the water–water interaction considering its avoidance of long-range Coulombic forces and high computational efficiency. The mW model is mathematically formulated via the Stillinger–Weber (SW) potential [54] as:

$$E_{\mathrm{w}} = \sum_{i}\sum_{j>i}\phi_2(r_{ij}) + \sum_{i}\sum_{j\neq i}\sum_{k>j}\phi_3(r_{ij}, r_{ik}, \theta_{ijk}) \tag{4}$$

$$\phi_2(r_{ij}) = A\varepsilon\left[B\left(\frac{\sigma}{r_{ij}}\right)^{p_{ij}} - \left(\frac{\sigma}{r_{ij}}\right)^{q_{ij}}\right]\exp\left(\frac{\sigma}{r_{ij} - a\sigma}\right) \tag{5}$$

$$\phi_3(r_{ij}, r_{ik}, \theta_{ijk}) = \lambda\varepsilon\left(\cos\theta_{ijk} - \cos\theta_0\right)^2 \exp\left(\frac{\gamma\sigma}{r_{ij} - a\sigma} + \frac{\gamma\sigma}{r_{ik} - a\sigma}\right) \tag{6}$$

where $r_{ij}$ is the distance between atom $i$ and atom $j$; $\theta_{ijk}$ is the angle between the vectors $r_{ij}$ and $r_{ik}$; the other parameters are constants: $A = 7.049556277$, $B = 0.6022245584$, $p_{ij} = 4$, $q_{ij} = 0$, $\gamma = 1.2$, $a = 1.8$, $\theta_0 = 109.47°$, $\lambda = 23.15$, $\sigma = 2.3925$ Å, and $\varepsilon = 6.189$ kcal/mol.

The solid–solid interaction was modeled as a harmonic potential. The harmonic potential was implemented by adding harmonic bonds between solid atoms to form a complete bonded FCC crystal structure as suggested by Luan and Robbins [32]. The harmonic potential ($E_{\mathrm{s}}$) can be mathematically expressed as:

$$E_{\mathrm{s}} = K(r_{ij} - r_0)^2 \tag{7}$$

where $K$ is the spring constant and calibrated as 6.2 kcal/mol, and $r_0 = 3.1$ Å is the equilibrium interaction distance.

The solid–water interaction was also modeled using the SW potential. The mathematical formulation is identical to that of the mW model [Eqs. (4–6)]. The parameters $\lambda$, $\sigma$, and $\varepsilon$ were changed to differ from the mW model. The values of $\lambda$ and $\sigma$ were calibrated as 0.0 and 3.2 Å by Moore et al. [38]. Herein, $\varepsilon$ indicates the magnitude of the solid–water interaction, i.e., wettability, and is referred as the solid–water interaction characteristic energy ($\varepsilon_{\mathrm{sw}}$). If the value of $\lambda$ is set as 0.0, the 3-body potential $\phi_3(r_{ij})$ vanishes, and consequently, the solid–water interaction is exclusively dominated by the 2-body potential $\phi_2(r_{ij})$, suggesting that $\varepsilon_{\mathrm{sw}}$ represents the magnitude of the van der Waals potential between the solid and water. The molecular component of the disjoining pressure can be obtained by integrating the 2-body potential $\phi_2(r_{ij})$ over the domain of interest [53], leading to the fact that the magnitude of the disjoining pressure is essentially proportional to the value of $\varepsilon_{\mathrm{sw}}$. The disjoining pressure is directly related to the wettability of the solid surface via the Derjaguin–Frumkin equation [11]. Therefore, the wettability of the solid surface could be tuned by adjusting the value of $\varepsilon_{\mathrm{sw}}$. In this study, $\varepsilon_{\mathrm{sw}}$ was varied from 0.2, 0.3 kcal/mol to 0.4 kcal/mol to investigate the influence of the solid substrate wettability. These values of $\varepsilon_{\mathrm{sw}}$ were calibrated with the aid of a trial–error process so that the contact angles of the solid in the molecular simulation approximate the contact angles of common soil minerals.

## 3.3 Simulation procedure

At first, the wettability of the solid substrate with different solid–water interaction characteristic energies ($\varepsilon_{\mathrm{sw}}$) was quantified with a series of MD simulations. For this purpose, a bulk water body, consisting of 672 water molecules, was deposited on the solid substrate, as illustrated in Fig. 3. This molecular system was equilibrated under a canonical ($NVT$) ensemble. A Nosé–Hoover thermostat was used to maintain the temperature at $T = 300$ K. The periodic boundary condition was applied in all the boundaries of the simulation cell. The simulation time was 5.0 ns with an integration time step of 5.0 fs. The time average density profiles of water droplets were computed from the molecular trajectories recorded in the last 2.0 ns. The contact angle was chosen as the indicator of the wettability and calculated from time average density profiles. A detailed

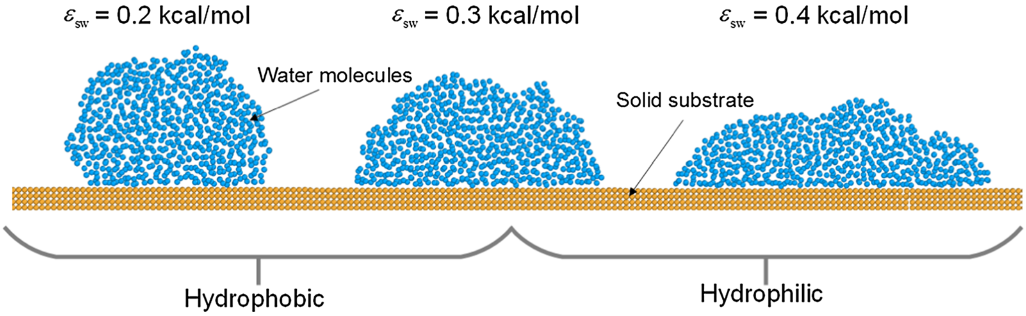

**Fig. 3** Snapshots of water droplet deposited on the solid substrate (yellow: solid atom; blue: water molecule) with different solid–water interaction characteristic energies ($\varepsilon_{sw}$) (color figure online)

description of the procedure for determining contact angles using MD can be found in Zhang et al. [62].

The water-pore system shown in Fig. 2 was used for the freezing simulation. As mentioned in Sect. 3.1, the pore diameter (*D*) was varied from 2.0 to 3.0 nm with an interval of 0.2 nm, while the solid–water interaction characteristic energy ($\varepsilon_{sw}$) was changed from 0.2, 0.3 kcal/mol to 0.4 kcal/mol. Consequently, there were a total of 18 cases for the freezing simulation. The water-pore system was equilibrated under an isothermal–isobaric (*NpT*) ensemble. The pressure was maintained at $P = 1.0$ atm using a Nosé–Hoover barostat. The system temperature (*T*) was first decreased from 250 to 50 K at a rate of 4 K/ns. Then, the system temperature was maintained at $T = 50$ K for 200 ns. The periodic boundary conditions were adopted for all the boundaries of the simulation cell. The integration time step was set as 10.0 fs. The equilibrium of MD simulations is confirmed by checking whether the total energy of the molecular system fluctuates around a specific value. The simulations were performed using the Large-scale Atomic/Molecular Massively Parallel Simulator (LAMMPS) distributed by the Sandia National Laboratories [42, 43] and visualized with the Open Visualization Tool (OVITO) [55].

## 4 Simulation results

### 4.1 Contact angles of solid substrates

The snapshots of molecular systems for determining contact angles are compared in Fig. 3. In general, the molecular system with $\varepsilon_{sw} = 0.2$ kcal/mol can be characterized as non-wetting or hydrophobic, whereas the molecular systems with $\varepsilon_{sw} = 0.3$ and 0.4 kcal/mol can be described as partial wetting or hydrophilic. The solid–water interaction characteristic energy ($\varepsilon_{sw}$) indicates the magnitude of the interaction energy between solid atoms and water molecules. The surface tension of water is one mechanism decreasing the system energy, while adsorption is the other. With a larger $\varepsilon_{sw}$, more energy will be dissipated when water molecules approach solid atoms, indicating that adsorption becomes a more efficient mechanism to reduce the system energy. There is a counterbalance between these two mechanisms, and the most stable or energetically favored state should maintain the minimum system energy among possible states. As a result, if the adsorption of water molecules to solids dissipates more energy than the surface tension, adsorption approach is more favored than the surface tension, and thus, the contact area between water molecules and the solid surface becomes larger. In a macroscopic viewpoint, this is interpreted as that the contact angle decreases, and the wettability of water on the solid substrate increases.

The contact angle was calculated from the time average density profiles as suggested by Zhang et al. [62]. The theoretical basis for this approach is the ergodic hypothesis. If a system is ergodic, the system will explore all the possible states in the phase space with a sufficient temporal scale ($\Delta t$). Then, macroscopic properties (e.g., temperature, density, thermal conductivity, contact angle, and Young's modulus) can be estimated from statistical weights of these states [56]. In the current study, the $\Delta t$ was calibrated as 1.0 ns, and the contact angles were estimated from the density profiles averaged over 1.0 ns. The boundary between water and vapor was determined using a fitting process suggested by Zhang et al. [62]. In Fig. 4, the red data points are the water–vapor boundary obtained using the fitting process. The contact angles were determined by further fitting these data points to the mathematical equation of circles. The determined contact angles are 129° for the molecular system with $\varepsilon_{sw} = 0.2$ kcal/mol; 88° for the molecular system with $\varepsilon_{sw} = 0.3$ kcal/mol; and 58° for the molecular system with $\varepsilon_{sw} = 0.4$ kcal/mol. The contact angles of the three types of solid substrates are comparable to the contact angles of common soil minerals [62] (e.g., 116° for muscovite; 36° for orthoclase; and 29° for α-quartz). Hence, it is reasonable to use these three types of solid substrates to represent common soil minerals with respect to the wettability.

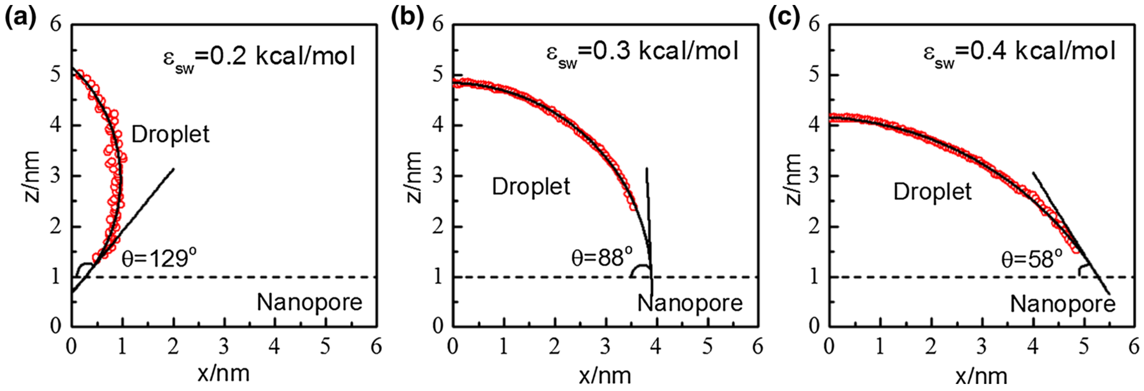

**Fig. 4** Determination of contact angles

## 4.2 Unfreezable threshold

Freezing process simulations were conducted using the 18 water-pore systems with different pore diameters or contact angles following the procedure introduced in Sect. 3.3. During the simulations, molecular trajectories were recorded every 100 ps. The main task of this study is to determine whether the pore water is freezable or not by decreasing the system temperature. For this purpose, a powerful crystal structure identification tool in the OVITO [55] was selected to identify ice structures in terms of coordination numbers. The amount of ice for all the simulation cases was determined by the OVITO using molecular positions recorded in the molecular trajectories.

The ice structure identification results revealed that water confined in the pores with a diameter smaller than 2.4 nm is unfreezable ($D < 2.4$ nm), and the contact angles of solid substrates do not exhibit a noticeable influence on the unfreezable threshold. The snapshots of water molecules confined in hydrophobic pores ($\varepsilon_{\mathrm{sw}} = 0.2$ kcal/mol, $\theta = 129°$) are presented in Fig. 5. The snapshots with too large or too small pores ($D > 2.4$ nm or $D = 2.0$ nm) are not shown as this study focus on the properties around the unfreezable threshold. In Fig. 5, a considerable amount of ice crystals can be observed in the $D = 2.4$ nm and $D = 2.6$ nm cases, while no ice crystal is seen in the $D = 2.2$ nm case. The water–vapor interface is convex, further proving that the solid substrate is hydrophobic. In Fig. 5a, the water molecules are arranged in sort of molecular orders albeit that no ice crystal is identified. These molecular orders should be classified as some kind of nanocrystals rather than regular ice crystal structures. This observation of nanocrystals is consistent with many other studies (e.g., Findenegg et al. [12], Koga et al. [21], and Shiomi et al. [49]). In Fig. 5b, c, some unfrozen water molecules are found in the cross-sectional view taken along the axis of pores. These unfrozen water molecules are adjacent to the solid surface and thus should be regarded as adsorptive water. Adsorptive water already exhibits some molecular orders due to the intense surface forces, making it harder to transform into ice. The free energy of this ordered adsorptive water can be extremely low [4], e.g., 8.62 kcal/mol lower than pure bulk water [64]. Even under extremely low temperatures, this ordered adsorptive water is still more energetically favored than ice. Consequently, the adsorptive water molecules remain “unfreezable” as they do not from ice structures.

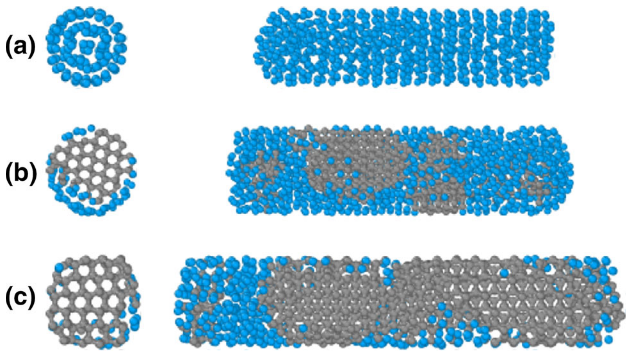

**Fig. 5** Snapshots of water molecules (blue: unfrozen water molecule; gray: ice) in hydrophobic pores ($\varepsilon_{\mathrm{sw}} = 0.2$ kcal/mol, $\theta = 129°$). Left part: cross-sectional view taken along the axis of pores; Right part: cross-sectional view taken perpendicular to the axis of pores (color figure online)

Figure 6 illustrates the snapshots of water molecules confined in hydrophilic pores ($\varepsilon_{\mathrm{sw}} = 0.4$ kcal/mol, $\theta = 58°$). Similar to the hydrophobic cases shown in Fig. 5, ice crystals coexist with unfrozen water molecules in the $D = 2.4$ nm and $D = 2.6$ nm cases, whereas only unfrozen water molecules are observed in the $D = 2.2$ nm case. However, the water–vapor interface is concave, differing from the convex cases in Fig. 5 and confirming the hydrophilicity of the solid. It is noted that the presence of the ice phase may change the local surface tension and thus alter the shape of the interface.

To further quantify the unfreezable threshold, the unfrozen water fraction was calculated and plotted versus

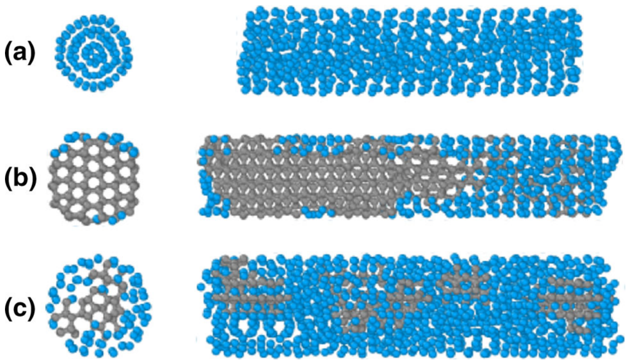

**Fig. 6** Snapshots of water molecules (blue: unfrozen water molecule; gray: ice) in hydrophilic pores ($\varepsilon_{\mathrm{sw}} = 0.4$ kcal/mol, $\theta = 58°$). Left part: cross-sectional view taken along the axis of pores; Right part: cross-sectional view taken perpendicular to the axis of pores (color figure online)

the pore diameter in Fig. 7. In smaller pores ($D = 2.0$ and 2.2 nm), the unfrozen water fraction is 1.0, indicating that all the pore water remains unfrozen. In larger pores ($D \geq 2.4$ nm), the unfrozen water fraction is lower than 1.0, suggesting that some pore water molecules formed ice structures. Nevertheless, no clear pattern was observed for the relationships between the unfrozen water fraction and pore properties. It should be noted that the amount of ice may not be accurate enough. A more precise determination of the amount of ice in the pores needs more simulation time including a crystal annealing process to make ice crystals compatible with their neighbors. The primary goal herein is to determine whether the water in the pores is freezable or not rather than how much water in the pores is frozen. Thus, the precise determination of the ice fraction is not included in the current study. Also, there is no correlation between the unfreezable threshold and pore wettability. Therefore, it can be concluded that the unfreezable threshold should locate between $D = 2.2$ nm and $D = 2.4$ nm and can be estimated to be $D = 2.3 \pm 0.1$ nm.

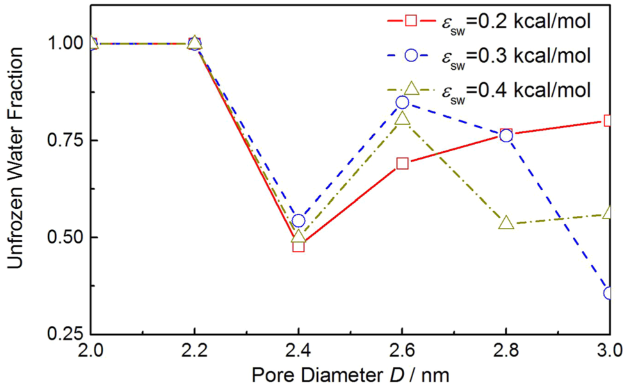

**Fig. 7** Variation of the unfrozen water fraction with the pore diameter ($D$)

## 5 Phase prediction model accounting for adsorption and unfreezable threshold

The melting temperature (or temperature depression)–pore diameter relationship is a crucial element in developing the BCC model. As mentioned in Sect. 1, there are mainly two approaches to obtain this relationship. The first one is derived by combining the Young–Laplace equation [Eq. (3)] and the Clapeyron equation [Eq. (2)] [29]. This approach is referred as the Young–Laplace–Clapeyron method in this study. For cylindrical pores, by substituting Eq. (3) into Eq. (2), the melting temperature can be estimated with the pore diameter as:

$$T_{\mathrm{m}} = T_0 \exp\left(\frac{4T_{\mathrm{s}} \cos \alpha}{-\rho_{\mathrm{w}} L_{\mathrm{a}} D}\right) \tag{8}$$

where $\alpha$ is the ice–water–solid interface contact angle (usually assumed to be 0°).

The second approach is based on the Gibbs–Thomson effect [57]. As for ice crystals with a small diameter, the high curvature will introduce excess free energy and thus alter the energy equilibrium between ice and water phases. As a result, the melting temperature of ice crystals is shifted to a lower value. This effect can be formulated via the Gibbs–Thomson equation as [15]:

$$T_{\mathrm{m}} = T_0\left(1 - \frac{2T_{\mathrm{s}}}{\rho_{\mathrm{i}} L_{\mathrm{a}} D}\right) \tag{9}$$

where $\rho_{\mathrm{i}}$ is the density of ice.

The two conventional methods are both based on the physical mechanism of surface tension, and both neglected adsorption and unfreezable threshold. The modified Gibbs–Thomson equation has frequently been used to predict the melting temperature of water confined in nano-size pores [12, 17, 38]. The modified Gibbs–Thomson equation can be written as [46]

$$T_{\mathrm{m}} = T_0 - \frac{2K_{\mathrm{GT}}}{D - 2d} \tag{10}$$

where $K_{\mathrm{GT}}$ and $d$ are constants to be determined by fitting to experimental results. In this study, the modified Gibbs–Thomson equation, where $K_{\mathrm{GT}}$ and $d$ are calibrated as 52.4 K nm and 0.6 nm by Findenegg et al. [12], respectively, was selected to account for adsorption. Obviously, the unfreezable threshold is not involved in the modified Gibbs–Thomson model, either. By introducing the unfreezable threshold to Eq. (10), a mathematical model for predicting the melting temperature incorporating adsorption and unfreezable threshold can be obtained as:

$$T_{\mathrm{m}} = \begin{cases} T_0 - \dfrac{2K_{\mathrm{GT}}}{D - 2d} & D > 2.3 \pm 0.1\,\mathrm{nm} \\ \text{Unfreezable} & D \leq 2.3 \pm 0.1\,\mathrm{nm} \end{cases} \tag{11}$$

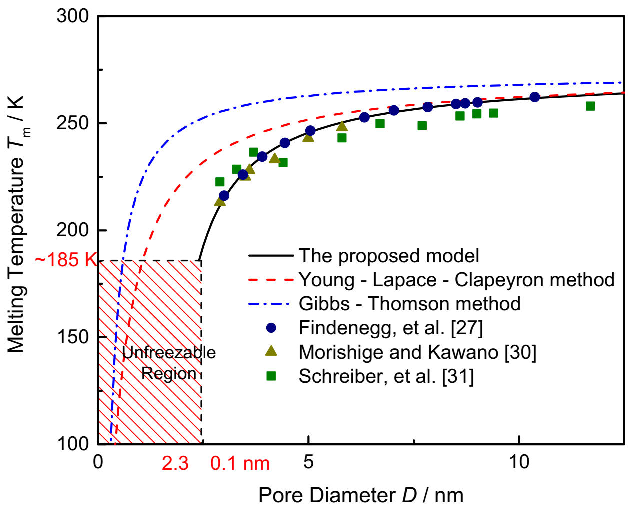

**Fig. 8** Comparisons of the proposed mathematical model for the relationship between the melting temperature ($T_m$) and the pore diameter ($D$) in cylindrical pores with two existing models and experimental results

The proposed mathematical model [Eq. (11)] was compared with the Young–Laplace–Clapeyron method [Eq. (8)], the Gibbs–Thomson method [Eq. (9)], and some nanoscale experimental results [12, 39, 46] in Fig. 8. In general, the proposed model provides a much more accurate prediction of the experimental results than the two conventional methods. The Gibbs–Thomson method usually estimates a considerably higher melting temperature than the Young–Laplace–Clapeyron method, the proposed model, and experimental results. In large pores ($D > 10$ nm), the Young–Laplace–Clapeyron method almost overlaps with the proposed model. However, the prediction by the proposed model is lower than the Young–Laplace–Clapeyron method in minuscule pores and closer to experimental results. The difference between the Young–Laplace–Clapeyron equation and experimental results increases with decreasing pore diameter, indicating that the contribution of adsorption becomes more manifest in smaller pores. Also, the existence of the unfreezable threshold is not reflected in the two conventional methods. The proposed model has provided a pathway to consider the two physical mechanisms missing in conventional models and therefore should be able to provide a more reasonable prediction of PCCs, especially in the low-temperature range.

## 6 Summary and conclusions

This study explored two physical mechanisms which are currently not considered but critical in frozen soils and their PCCs, especially in the low-temperature range: unfreezable threshold and adsorption, based on free energy concepts. A series of MD simulations were conducted to investigate the unfreezable threshold. Based on the simulation results and the modified Gibbs–Thomson equation, an explicit mathematical equation was proposed to predict the melting temperature in cylindrical pores accounting for the two missing physical mechanisms. Major findings and conclusions are summarized below:

1. Adsorption tends to further depress the melting temperature of pore water confined in small pores in addition to capillarity. In minuscule pores, the intense surface forces arrange the pore water molecules into regular molecular orders, leading to the existence of an unfreezable threshold (pore size or temperature), below which pore water will not freeze. The unfreezable threshold is absent in the conventional methods for predicting the phase behavior of pore water.
2. A series of MD simulations was conducted to estimate the unfreezable threshold accurately. Based on the simulation results, the unfreezable threshold is estimated as $D = 2.3 \pm 0.1$ nm. In addition, the unfreezable threshold is found to be insensitive to the wettability of the solid substrates.
3. Compared with other methods and experimental results, the Gibbs–Thomson method tends to overestimate the melting temperature. The proposed model is approximately equivalent to the Young–Laplace–Clapeyron method in the pores with a diameter $D > 10$ nm. In the small pores, the proposed model provides estimates that are much closer to the existing experimental results than the Young–Laplace–Clapeyron method. In addition, the prediction error of the Young–Laplace–Clapeyron method increases with a decreasing pore diameter.

**Acknowledgements** The financial support from the National Science Foundation (NSF CMMI 1562522) and the Michigan Space Grant Consortium by National Aeronautics and Space Administration (Grant No. MSGC1311039) is gratefully acknowledged. We also acknowledge Superior, a high-performance computing cluster at Michigan Technological University, for providing computational resources to fulfill this study.

## References

1. Alba-Simionesco C, Coasne B, Dosseh G, Dudziak G, Gubbins K, Radhakrishnan R, Sliwinska-Bartkowiak M (2006) Effects of confinement on freezing and melting. J Phys Condens Matter 18(6):R15
2. Amarasinghe PM, Anandarajah A (2011) Influence of fabric variables on clay–water–air capillary meniscus. Can Geotech J 48:987–995
3. Anandarajah A, Amarasinghe PM (2011) Microstructural investigation of soil suction and hysteresis of fine-grained soils. J Geotech Geoenviron Eng 138(1):38–46

4. Baker R, Frydman S (2009) Unsaturated soil mechanics: critical review of physical foundations. Eng Geol 106(1):26–39
5. Berendsen HJ, Postma JP, van Gunsteren WF, Hermans J (1981) Interaction models for water in relation to protein hydration. In: Intermolecular forces. Springer, Berlin, pp 331–342
6. Berendsen HJC, Grigera JR, Straatsma TP (1987) The missing term in effective pair potentials. J Phys Chem-Us 91(24):6269–6271. https://doi.org/10.1021/j100308a038
7. Borja RI (2013) Plasticity: modeling and computation. Springer, Berlin
8. Borja RI, Song X, Wu W (2013) Critical state plasticity. Part VII: triggering a shear band in variably saturated porous media. Comput Method Appl Mech Eng 261:66–82
9. Cahn J, Dash J, Fu H (1992) Theory of ice premelting in monosized powders. J Cryst Growth 123(1–2):101–108
10. Cheng SF, Robbins MO (2014) Capillary adhesion at the nanometer scale. Phys Rev E 89(6):62402. https://doi.org/10.1103/physreve.89.062402
11. Churaev NV, Derjaguin BV, Muller VM (2013) Surface forces. Springer, New York
12. Findenegg GH, Jähnert S, Akcakayiran D, Schreiber A (2008) Freezing and melting of water confined in silica nanopores. Chem Phys Chem 9(18):2651–2659
13. Gonzalez Solveyra E, De La Llave E, Scherlis DA, Molinero V (2011) Melting and crystallization of ice in partially filled nanopores. J Phys Chem B 115(48):14196–14204
14. Hockney RW, Eastwood JW (1988) Computer simulation using particles. CRC Press, Boca Raton
15. Ishizaki T, Maruyama M, Furukawa Y, Dash J (1996) Premelting of ice in porous silica glass. J Cryst Growth 163(4):455–460
16. Iwata S, Tabuchi T, Warkentin BP (1995) Soil–water interactions: mechanisms and applications, vol 2. Marcel Dekker, Inc, New York
17. Jähnert S, Chavez FV, Schaumann G, Schreiber A, Schönhoff M, Findenegg G (2008) Melting and freezing of water in cylindrical silica nanopores. Phys Chem Chem Phys 10(39):6039–6051
18. Jorgensen WL, Tirado-Rives J (2005) Potential energy functions for atomic-level simulations of water and organic and biomolecular systems. Proc Natl Acad Sci USA 102(19):6665–6670
19. Katti DR, Schmidt SR, Ghosh P, Katti KS (2007) Molecular modeling of the mechanical behavior and interactions in dry and slightly hydrated sodium montmorillonite interlayer. Can Geotech J 44(4):425–435. https://doi.org/10.1139/T06-127
20. Katti DR, Srinivasamurthy L, Katti KS (2015) Molecular modeling of initiation of interlayer swelling in Na-montmorillonite expansive clay. Can Geotech J 52:1385–1395
21. Koga K, Gao G, Tanaka H, Zeng XC (2001) Formation of ordered ice nanotubes inside carbon nanotubes. Nature 412(6849):802–805
22. Konrad J-M, Morgenstern NR (1980) A mechanistic theory of ice lens formation in fine-grained soils. Can Geotech J 17(4):473–486
23. Konrad J-M, Morgenstern NR (1981) The segregation potential of a freezing soil. Can Geotech J 18(4):482–491
24. Koopmans RWR, Miller R (1966) Soil freezing and soil water characteristic curves. Soil Sci Soc Am J 30(6):680–685
25. Kurylyk BL, Watanabe K (2013) The mathematical representation of freezing and thawing processes in variably-saturated, non-deformable soils. Adv Water Resour 60:160–177
26. Laplace PS (1806) Supplement to book 10 of Mecanique Celeste. Crapelet, Courcier, Bachelier
27. Liao M, Lai Y, Liu E, Wan X (2017) A fractional order creep constitutive model of warm frozen silt. Acta Geotech 12(2):377–389
28. Likos WJ, Yao J (2014) Effects of constraints on van Genuchten Parameters for modeling soil–water characteristic curves. J Geotech Geoenviron 140(12):06014013
29. Liu Z, Yu X (2013) Physically based equation for phase composition curve of frozen soils. Transp Res Rec J Transp Res Board 2349:93–99
30. Liu Z, Sun Y, Yu XB (2012) Theoretical basis for modeling porous geomaterials under frost actions: a review. Soil Sci Soc Am J 76(2):313–330
31. Lu N, Likos WJ (2004) Unsaturated soil mechanics. Wiley, New York
32. Luan B, Robbins MO (2005) The breakdown of continuum models for mechanical contacts. Nature 435(7044):929–932
33. Ma L, Qi J, Yu F, Yao X (2016) Experimental study on variability in mechanical properties of a frozen sand as determined in triaxial compression tests. Acta Geotech 11(1):61–70
34. Martínez L, Andrade R, Birgin EG, Martínez JM (2009) PACKMOL: a package for building initial configurations for molecular dynamics simulations. J Comput Chem 30(13):2157–2164. https://doi.org/10.1002/jcc.21224
35. Mitchell JK, Soga K (2005) Fundamentals of soil behavior. Wiley, New York
36. Molinero V, Moore EB (2008) Water modeled as an intermediate element between carbon and silicon†. J Phys Chem B 113(13):4008–4016
37. Moore EB, Molinero V (2011) Structural transformation in supercooled water controls the crystallization rate of ice. Nature 479(7374):506–508
38. Moore EB, Allen JT, Molinero V (2012) Liquid-ice coexistence below the melting temperature for water confined in hydrophilic and hydrophobic nanopores. J Phys Chem C 116(13):7507–7514
39. Morishige K, Kawano K (1999) Freezing and melting of water in a single cylindrical pore: the pore-size dependence of freezing and melting behavior. J Chem Phys 110(10):4867–4872
40. Noy-Meir I, Ginzburg B (1967) An analysis of the water potential isotherm in plant tissue. Aust J Biol Sci 22(1):35–52
41. Painter SL, Karra S (2014) Constitutive model for unfrozen water content in subfreezing unsaturated soils. Vadose Zone J 13(4):1–8
42. Plimpton S (1995) Fast parallel algorithms for short-range molecular-dynamics. J Comput Phys 117(1):1–19. https://doi.org/10.1006/jcph.1995.1039
43. Plimpton S, Crozier P, Thompson A (2007) LAMMPS-large-scale atomic/molecular massively parallel simulator, vol 18. Sandia National Laboratories, Livermore
44. Schmidt R, Hansen EW, Stoecker M, Akporiaye D, Ellestad OH (1995) Pore size determination of MCM-51 mesoporous materials by means of 1H NMR spectroscopy, $N_2$ adsorption, and HREM: a preliminary study. J Am Chem Soc 117(14):4049–4056
45. Schofield R (1935) The pF of the water in soil. In: Transactions of 3rd international congress of soil science, pp 37–48
46. Schreiber A, Ketelsen I, Findenegg GH (2001) Melting and freezing of water in ordered mesoporous silica materials. Phys Chem Chem Phys 3(7):1185–1195
47. Schuur EA, Bockheim J, Canadell JG, Euskirchen E, Field CB, Goryachkin SV, Hagemann S, Kuhry P, Lafleur PM, Lee H (2008) Vulnerability of permafrost carbon to climate change: implications for the global carbon cycle. Bioscience 58(8):701–714
48. Sheng D, Zhang S, Yu Z, Zhang J (2013) Assessing frost susceptibility of soils using PCHeave. Cold Reg Sci Technol 95:27–38
49. Shiomi J, Kimura T, Maruyama S (2007) Molecular dynamics of ice-nanotube formation inside carbon nanotubes. J Phys Chem C 111(33):12188–12193

50. Song X, Borja RI (2014) Mathematical framework for unsaturated flow in the finite deformation range. Int J Numer Meth Eng 97(9):658–682
51. Song X, Borja RI (2014) Finite deformation and fluid flow in unsaturated soils with random heterogeneity. Vadose Zone J 13(5)
52. Spaans EJ, Baker JM (1996) The soil freezing characteristic: its measurement and similarity to the soil moisture characteristic. Soil Sci Soc Am J 60(1):13–19
53. Starov VM, Velarde MG, Radke CJ (2007) Wetting and spreading dynamics, vol 138. CRC Press, Boca Raton
54. Stillinger FH, Weber TA (1985) Computer simulation of local order in condensed phases of silicon. Phys Rev B 31:5262
55. Stukowski A (2010) Visualization and analysis of atomistic simulation data with OVITO–the Open Visualization Tool. Modell Simul Mater Sci Eng 18(1):015012
56. Tadmor EB, Miller RE (2011) Modeling materials: continuum, atomistic and multiscale techniques. Cambridge University Press, Cambridge
57. Watanabe K, Flury M (2008) Capillary bundle model of hydraulic conductivity for frozen soil. Water Resour Res 44(12)
58. Webb SW (2000) A simple extension of two-phase characteristic curves to include the dry region. Water Resour Res 36(6):1425–1430
59. Xu G, Wu W, Qi J (2016) Modeling the viscous behavior of frozen soil with hypoplasticity. Int J Numer Anal Met 40(15):2061–2075
60. Young T (1805) An essay on the cohesion of fluids. In: Philosophical Transactions of the Royal Society of London, pp 65–87
61. Zhang S, Sheng D, Zhao G, Niu F, He Z (2015) Analysis of frost heave mechanisms in a high-speed railway embankment. Can Geotech J 53(999):1–10
62. Zhang C, Liu Z, Deng P (2016) Contact angle of soil minerals: a molecular dynamics study. Comput Geotech 75:48–56. https://doi.org/10.1016/j.compgeo.2016.01.012
63. Zhang C, Liu Z, Deng P (2016) Atomistic-scale investigation of effective stress principle of saturated porous materials by molecular dynamics. Geophys Res Lett 43(19):10257–210265. https://doi.org/10.1002/2016gl070101
64. Zhang C, Dong Y, Liu Z (2017) Lowest matric potential in quartz: metadynamics evidence. Geophys Res Lett 44(4):1706–1713. https://doi.org/10.1002/2016GL071928
65. Zhang C, Liu Z, Dong Y (2017) Effects of adsorptive water on the rupture of nanoscale liquid bridges. Appl Clay Sci 146:487–494. https://doi.org/10.1016/j.clay.2017.07.002
66. Zhao X, Zhou G, Lu G (2017) Strain responses of frozen clay with thermal gradient under triaxial creep. Acta Geotech 12(1):183–193